Vibrational Spectroscopy of a Picosecond, Structurally-Restricted Intermediate Containing a Seven-Membered Ring in the Room-Temperature Photoreaction of an Artificial Rhodopsin

F. Jäger,[†] Jihong Lou,[‡] Koji Nakanishi,[‡] L. Ujj,[†] and G. H. Atkinson*,[†]

Contribution from the Department of Chemistry and Optical Science Center, University of Arizona, Tucson, Arizona 85721, and Department of Chemistry, Columbia University, New York, New York 10027

Abstract: The vibrational degrees of freedom of the only photophysical intermediate formed during the photoreaction of an artificial rhodopsin (Rh) containing a retinal with a seven-membered ring blocking 11-*cis* isomerization (Rh7.10) is measured via picosecond time-resolved coherent anti-Stokes Raman spectroscopy (PTR/CARS). PTR/CARS spectra are recorded with time delays ranging from 0 (8-ps cross correlation time) to 50 ps following the 3-ps, 500-nm excitation of Rh7.10. For time delays between 0 and 15 ps, an intermediate (P7.10) with a vibrational structure distinct from that of the ground electronic state Rh7.10 is observed. Although the formation time of P7.10 cannot be resolved from these PTR/CARS data, it is estimated to be ~1 ps (i.e., slower than the 200-fs process proposed for native Rh). P7.10 completely reforms Rh7.10 with a decay time estimated to be ~5−6 ps from the increasing intensities (via amplitudes from third-order, nonlinear susceptibility ($\chi^{(3)}$) analysis) in three major PTR/CARS features (at 955, 1235, and 1551 cm^{-1}). The structural changes occurring as P7.10 is formed can be derived from vibrational mode assignments in the PTR/CARS spectra such as the 955-cm^{-1} band assigned as the HC$_{11}$=C$_{12}$H hydrogen-out-of-plane (HOOP) mode (shifts to 946 cm^{-1}, increases intensity, and broadens its width in P7.10) and the 1551-cm^{-1} band assigned as the C=C stretching mode (shifts to 1546 cm^{-1} in P7.10). These PTR/CARS data show that incorporation of an 11-ene, seven-membered ring into the retinal chromophore permits some flexibility for torsional motion around the C$_{11}$=C$_{12}$ bond and within the seven-membered ring, but does not allow considerable out-of-plane motion near the Schiff base or the β-ionone ring. The $\chi^{(3)}$ analysis of these PTR/CARS data demonstrates that a series of structurally-distinct retinals having slightly different C$_{11}$=C$_{12}$ torsional, out-of-plane motion appear (collectively P7.10). The amplitudes and shifts in frequency of the PTR/CARS vibrational features change on a time scale comparable to that of vibrational relaxation in native Rh. The structural variations observed within P7.10 are located at/near the C$_{11}$=C$_{12}$ bond (reactive in native Rh^{RT}, but nonreactive in R7.10) and the degree of π-electron energy delocalization throughout the retinal changes. This latter phenomenon is reflected in the different electronic phase factor (Θ) found in the $\chi^{(3)}$ analysis of the PTR/CARS data. The relationship(s) of the P7.10 structure to that of the C$_{11}$=C$_{12}$ reaction coordinates in native Rh is discussed.

Introduction

The visual process in most vertebrates, and in some invertebrates, is based on the light activation of rhodopsin (Rh) which converts absorbed optical energy into an electrical (synaptic nerve) response via activating the G-protein transducin at the surface of the transmembrane Rh protein.[1] These transduction processes include the hyperpolarization of the rod outer segment (ROS). Extensive research has been conducted to elucidate the molecular processes by which Rh converts the initial optical information (absorbed light) available from even a single photon into the distinct structural/conformational species that form an activated Rh state.

Specifically, after formation of the Franck−Condon (FC) excited electronic state by optical absorption in Rh, energy is thought to coherently propagate along the polyene chain starting at the protonated Schiff base and dissipating into ground-state vibrational modes.[2] The ultrafast (200 fs), 11-*cis* to all-*trans* isomerization of the retinal chromophore[3] is regarded as a key molecular step for energy storage/transduction in native Rh and is associated with a 60-cm^{-1} torsional mode observed within the first few picoseconds after laser excitation.[4] Recently, a model has been proposed which assumes that the 200-fs, 11-*cis* isomerization process competes successfully with vibrational dephasing.[5]

The ultrafast (femto/picosecond) Rh photochemistry associated with vision has been examined extensively by transient absorption[3,4,6,7] and fluorescence[8−11] measurements. Such transient absorption/fluorescence experiments have also been

* To whom correspondence should be addressed.
† University of Arizona.
‡ Columbia University.
⊗ Abstract published in *Advance ACS Abstracts,* December 15, 1997.
(1) Aaronson, S. A.; Benkovic, S. J.; Cozzarelli, N. R.; McKnight, S. L.; Prusiner, S. B.; Rancaniello, V. R.; Stryer, L.; Tilghman, S. M. *Harvey Lectures*; Wiley-Liss, Inc.: New York, 1971; p 87.

(2) Buda, F.; Degroot, H. J. M.; Bifone, A. *Phys. Rev. Lett.* **1996,** *77,* 4474−4477.
(3) Schoenlein, R. W.; Peteanu, L. A.; Mathies, R. A.; Shank, C. V. *Science* **1991,** *254,* 412.
(4) Wang, Q.; Schoenlein, R. W.; Peteanu, L. A.; Mathies, R. A.; Shank, C. V. *Science (Washington, D.C.)* **1994,** *266,* 422.
(5) Kochendoerfer, G. G.; Mathies, R. A. *Isr. J. Chem.* **1995,** *35,* 211.

3740 *J. Am. Chem. Soc., Vol. 120, No. 15, 1998*

Jäger et al.

conducted on (i) all-*trans* and 13-*cis*-retinal with protonated Schiff bases (PSB)[12,13] in solution, (ii) structurally-modified, 11-*cis*-retinals containing an 11-ene carbocyclic 8/9-ring encompassing the C_{10} to C_{13} bonds,[9] and (iii) Rh regenerated with five- to eight-membered rings spanning C_{10} through C_{13} (i.e., Rh5.10, Rh7.10, and Rh8.10 where for example Rh5.10 denotes Rh containing a five-membered ring starting at C_{10}).[8,14−17] Another recent study examines steric interactions of the excited-state isomerization via 13-demethyl rhodopsin and 10-methyl-13-demethyl rhodopsin.[18] Other studies report the photochemical quantum yields associated with these species.[11,19,20] Further investigations attempt to elucidate the energy storage/transduction mechanism via nanosecond transient absorption spectroscopy on other artificial Rh pigments[21−24] or studies on artificial retinals.[25,26]

An at least partial understanding of the ultrafast, 11-*cis* isomerization process has emerged from these studies that links the structural changes underlying isomerization with the inherent retinal geometry and the interactions (e.g., steric and/or electrostatic) between retinal and the apoprotein (opsin). Specifically, the steric hindrance between the hydrogen at C_{10} and the methyl group at C_{13} is considered the prime candidate for the driving force in the 11-*cis* to 11-*trans* isomerization.[5] Coulombic interactions between charges on the retinal and the protein (e.g., involving the counterion Glu-113) may also play a role in the ultrafast, 11-*cis* isomerization.

No vibrational data on the primary structural event(s) underlying 11-*cis* isomerization in vision have been available until recently. The initial work encompasses a significant number of the vibrational degrees of freedom in the room-temperature Rh (Rh^{RT}) photoreaction and utilizes picosecond time-resolved coherent anti-Stokes Raman scattering (PTR/
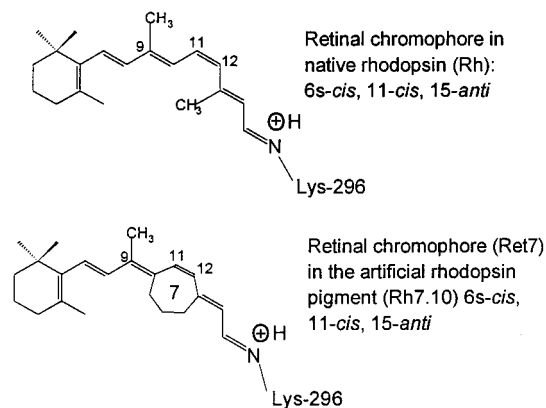
Figure 1. Retinal structures of (top) the 11−*cis* retinal in native Rh^{RT} and (bottom) the 11-*cis*-retinal containing a seven-membered ring bridging the C_{10} to C_{13} (i.e., locked 11-*cis*-structure) in the artificial Rh pigment, Rh7.10.

CARS) to examine the bathorhodopsin (batho^{RT}) and lumirhodopsin (lumi^{RT}) intermediates.[27,28,35] Nonlinear, third-order susceptibility ($\chi^{(3)}$) analyses of these high-quality (S/N) CARS data lead to band frequency measurements in batho^{RT} of $\pm$ 2 cm^{-1}. Recent experimental improvements in the PTR/ CARS techniques have directly reduced the uncertainties found in the earliest work[27] and provide a unique set of parameters (band origin positions, amplitudes, and bandwidths) describing the vibrational degrees of freedom of Rh^{RT} and batho^{RT} throughout the 700−1700 cm^{-1} range.

In this study, attention is given to measuring the vibrational degrees of freedom associated with an artificial Rh pigment obtained by regeneration of opsin with a seven-membered ring blocking the *cis* geometry via a carbon side chain extending from C_{10} to C_{13} (Rh7.10) (Figure 1). In Rh7.10, isomerization around C_{11}=C_{12} is blocked and no enzymatic activity is reported.[29,30] Since the absorption maxima and circular dichroism extrema measured for Rh7.10 at 490 nm ($\Delta\epsilon$ + 16.9)/488 nm and 330 nm ($\Delta\epsilon$ + 14.3)[31] are similar to those measured for native Rh at 500 nm and 337 nm ($\Delta\epsilon$ + 9.8)/480 nm ($\Delta\epsilon$ + 2.8), the environments of the respective protein-binding pockets are also considered to be similar. A photoproduct with a red-shifted absorption maximum (580 nm) is observed following the 21-ps, 532-nm excitation of Rh7.10 (a 44-ps lifetime for the intermediate is reported).[8] The 580-nm species may have properties, including its vibrational structure, analogous to those of the initial photoproduct (photo^{RT}) proposed to appear in the native Rh^{RT} photoreaction. The PTR/CARS data reported here (measured following 3-ps, 500-nm excitation of Rh7.10) confirm the presence of a species with a red-shifted absorption spectrum via changes in the electronic phase factor (Θ) and the frequency decrease ($\sim$5 cm^{-1}) of the C=C stretching band. This species is designated P7.10. The $\chi^{(3)}$ fit parameter derived for P7.10 from the PTR/CARS data yields a value for Θ corresponding to a 520−525-nm absorption maximum. The 500−525-nm absorption maximum assignable to P7.10 yields a smaller red shift (relative to Rh7.10) than that derived from picosecond transient absorption (PTA) measurements.[8] The red shift in

(6) Peteanu, L. A.; Schönlein, R. W.; Wang, Q.; Mathies, R. A.; Shank, C. V. *Proc. Natl. Acad. Sci. U.S.A.* **1993**, *90*, 11762.

(7) Yan, M.; Manor, D.; Weng, G.; Chao, H.; Rothberg, L.; Jedju, T. M.; Alfano, R. R.; Callender, R. H. *Proc. Natl. Acad. Sci. U.S.A.* **1991**, *88*, 9809.

(8) Kandori, H.; Matuoka, S.; Shichida, Y.; Yoshizawa, T.; Ito, M.; Tsukida, K.; Balogh-Nair, V.; Nakanishi, K. *Biochemistry* **1989**, *28*, 6460.

(9) Mcgarry, P. F.; Cheh, J.; Ruizsilva, M.; Hu, S. H.; Nakanishi, K.; Turro, N. J. *J. Phys. Chem.* **1996**, *100*, 646.

(10) Doukas, A. G.; Junnarkar, M. R.; Alfano, R. R.; Callender, R. H.; Kakitani, T.; Honig, B. *Proc. Natl. Acad. Sci. U.S.A.* **1984**, *81*, 4790.

(11) Kochendoerfer, G. G.; Mathies, R. A. *J. Phys. Chem.* **1996**, *100*, 14526.

(12) Logunov, S. L.; Long, L.; El-Sayed, M. A. *J. Phys. Chem.* **1996**, *100*, 18586.

(13) Hamm, P.; Zurek, M.; Roschinger, T.; Patzelt, H.; Oesterhelt, D.; Zinth, W. *Chem. Phys. Lett.* **1996**, *263*, 613.

(14) Mizukami, T.; Kandori, H.; Shichida, Y.; Chen, A.-H.; Derguini, F.; Caldwell, C. G.; Bigge, C. F.; Nakanishi, K.; Yoshizawa, T. *Proc. Natl. Acad. Sci. U.S.A.* **1993**, *90*, 4072.

(15) Buchert, J.; Stefancic, V.; Doukas, A. G.; Alfano, R. R.; Callender, R. H.; Pande, J. *Biophys. J.* **1983**, *43*, 279.

(16) Kandori, H.; Sasabe, H.; Nakanishi, K.; Yoshizawa, T.; Mizukami, T.; Shichida, Y. *J. Am. Chem. Soc.* **1996**, *118*, 1002.

(17) Kandori, H.; Katsuta, Y.; Ito, M.; Sasabe, H. *J. Am. Chem. Soc.* **1995**, *117*, 2669.

(18) Kochendoerfer, G. G.; Verdegem, P. J. E.; van der Hoef, I.; Lugtenburg, J.; Mathies, R. A. *Biochemistry* **1996**, *35*, 16230.

(19) Hurley, J. B.; Ebrey, T. G.; Honig, B.; Ottolenghi, M. *Nature* **1977**, *270*, 540.

(20) Shichida, Y.; Kropf, A.; Yoshizawa, T. *Biochemistry* **1981**, *20*, 1962.

(21) Randall, C. E.; Lewis, J. W.; Hug, S. J.; Björling, S. C.; Eisner-Shanas, I.; Friedman, N.; Ottolenghi, M.; Sheves, M.; Kliger, D. S. *J. Am. Chem. Soc.* **1991**, *113*, 3473.

(22) Hug, S. J.; Lewis, J. W.; Einterz, C. M.; Thorgeirsson, T. E.; Kliger, D. S. *Biochem.* **1990**, *29*, 1475.

(23) Kliger, D. S.; Lewis, J. W. *Isr. J. Chem.* **1995**, *35*, 289.

(24) Lewis, J. W.; Pinkas, I.; Sheves, M.; Ottolenghi, M.; Kliger, D. S. *J. Am. Chem. Soc.* **1995**, *117*, 918.

(25) Livnah, N.; Sheves, M. *J. Am. Chem. Soc.* **1993**, *115*, 351.

(26) Baasov, T.; Friedman, N.; Sheves, M. *Biochemistry* **1987**, *26*, 3210.

(27) Popp, A.; Ujj, L.; Atkinson, G. H. *Proc. Natl. Acad. Sci. U.S.A.* **1996**, *93*, 372.

(28) Jäger, F.; Ujj, L.; Atkinson, G. H. *J. Am. Chem. Soc.* **1997**, *119*, 12610.

(29) Crouch, R.; Nodes, B. R.; Perlman, J. I.; Pepperberg, D. R.; Akita, H.; Nakanishi, K. *Invest. Ophthalmol. Visual Sci.* **1984**, *25*, 419.

(30) Zankel, T.; Ok, H.; Johnson, R.; Chang, C. W.; Sekiya, N.; Naoki, H.; Yoshihara, K.; Nakanishi, K. *J. Am. Chem. Soc.* **1990**, *112*, 5387.

(31) Akita, H.; Tanis, S. P.; Adams, M.; Balogh-Nair, V.; Nakanishi, K. *J. Am. Chem. Soc.* **1980**, *102*, 6370.

absorption derived from PTR/CARS data, however, is comparable to that found for batho^{RT} via PTA data.[28] The major PTR/CARS feature assignable to P7.10 is the 955-cm^{-1} HOOP band which, relative to the analogous Rh7.10 bands, decreases position by >8 cm^{-1} and increases in bandwidth by more than a factor of 3. The measured characteristics of the 955-cm^{-1} feature suggest a significant twisting of the retinal backbone structure when P7.10 is formed. Essentially no spectral changes appear in the fingerprint region, indicating that the C—C=C backbone retinal structure, including that associated with the 11-*cis* geometry, remains unchanged during the formation and decay of P7.10. By contrast, the observation of a substantial shift of the 955-cm^{-1} band in the PTR/CARS measurements indicates significant motion in the seven-membered ring part (including the C$_{11}$=C$_{12}$ bond) of the retinal.

Experimental Section

1. Preparation of the Structurally-Modified Pigment. Bovine ROSs are prepared from bovine retinas obtained within 24 h of their availability (W. Lawson Co., Lincoln, NE). Isolation of ROS is performed at 4 °C under low intensity, red (>680 nm) light following a standard procedure.[31] Sucrose solutions are prepared with isotonic buffer (buffer A: 10 mM Tris, pH 8.0, 60 mM KCl, 30 mM NaCl, 2 mM MgCl$_2$, 1 mM dithiothreitol (DTT)). Retinas (typically 200) are gently shaken for 1 min in 160 mL of a 35% (w/v) sucrose solution and then centrifuged for 10 min at 3000g. The resultant pellets are resuspended in a 35% (w/v) sucrose solution (160 mL) and centrifuged a second time. The two supernatant solutions are combined and diluted with buffer A to obtain a 26% (w/v) sucrose solution. After centrifugation at 27000g for 30 min, the crude ROS pellets are resuspended gently in a 26% (w/v) sucrose solution and placed on a 26−35%, discontinuous gradient. Centrifugation in a swinging-bucket rotor (SW 28) at 23 000 rpm for 4 h produces a thin layer of purified ROS which is resuspended with a pipet and washed twice with buffer A.

The purified ROS is resuspended in buffer B (buffer B: 10 mM HEPES, pH 7.0, 50 μM DTPA, 0.1 mM PMSF, 1 mM DTT) with 100 mM hydroxylamine to obtain a concentration of 0.5 OD ROS/mL, a solution which is bleached under room light for 3 h in an ice bath. Hydroxylamine is removed by washing with buffer B five times. The opsin is subsequently resuspended in 150 mL of buffer B in preparation for the Rh binding step.

The structurally-modified retinal (Figure 1, Ret7) is synthesized by methods described previously.[31] The Ret7 preparation includes purification by HPLC in order to obtain one isomer having an 11-*cis*-retinal geometry (as confirmed by NOE experiments). The opsin suspension (prepared separately, *vide supra*) is combined under controlled light conditions in an approximately 1.5 molar ratio with Ret7 which is dissolved in ethanol. The mixed solution is incubated for 2 h at 20 °C and subsequently for 24 h at 4 °C to produce the artificial Rh pigment, Rh7.10. The mixture is washed five times with buffer B and resuspended in about 50 mL of buffer B for PTR/CARS measurements. The total amount of Rh7.10 sample can be estimated from ultraviolet/visible absorption spectra to be about 150 OD. Unlike BR, no light or dark adaptation of Rh has been reported. The Rh7.10 pigment obtained by reconstitution, therefore, contains only one isomer (11-*cis*-retinal) and is stable in normal light conditions.[31]

A typical sample volume required to record one PTR/CARS spectrum is 25−30 mL. To improve the S/N, two PTR/CARS spectra from consecutive measurements are summed. Since no Rh7.10 sample degradation is observed over the several minutes required to record two PTR/CARS spectra, the band amplitudes and line shapes can be quantitatively added.

2. PTR/CARS Experiment. Since detailed descriptions of the laser instrumentation, experimental procedure, and the $\chi^{(3)}$ analysis methodology underlying these PTR/CARS measurements are given elsewhere,[32−35]

only a brief description is provided here. A mode-locked Nd:YLF laser (Coherent, Antares 76 YLF) generates 30-ps pulses at 1054 nm which are used to generate second and third harmonic (Coherent 7950 THG) outputs from BBO (527 nm) and LBO (351 nm) crystals. The 527- and 351-nm radiation is used to pump three, independently controlled dye lasers (Coherent, model 700). Each dye laser is equipped with a cavity dumper (Coherent, models 7210 and 7220), all three of which are synchronized to the 76-MHz repetition rate of the Nd:YLF mode locker. Typically, the laser system is operated at a 400-kHz repetition rate to match the experimental conditions selected to form the liquid sample jet. Specifically, the velocity in the 400-μm, square glass nozzle is adjusted to >12 m/s to ensure a complete replacement of the sample volume between sets of pump and CARS laser pulses. Such volume replacement is determined by the beam waist of the pump beam (20 μm) and the 400-kHz laser repetition rates. A sample geometry of two, parallel liquid jet nozzles is chosen so that the nonresonant background signal (water) is measured simultaneously with the CARS signal from the Rh7.10 sample. This is achieved by projecting the beams of the reference and sample jets onto two, vertically-separated, parallel stripes of the liquid-nitrogen-cooled, CCD array (Princeton Instruments LN/CCD-1024-F/1UV) attached to a triple monochromator (Spex triplemate) selected to wavelength disperse the CARS signals.

Procedurally, the PR/CARS spectrum from Rh7.10 is recorded under conditions where the sample concentration remains constant. A PTR/CARS spectrum from the optically-excited Rh7.10 sample is subsequently recorded. This procedure is repeated in alternating order to ensure that the long-term decrease in Rh7.10 concentration does not disproportionately affect the results.

Rh7.10 is excited with a 500-nm, 3-ps (ω_p) laser pulse (2.5 mW or 7.5 nJ/pulse), thereby starting the Rh7.10 photoreaction. Two probe lasers, ω_1 (600 nm, 2.5 nJ) and ω_s (640 or 653 nm, 4.5 nJ), are used to generate CARS signals at 565 nm (HOOP and fingerprint regions) and 555 nm (fingerprint and C=C regions), respectively. An 8-ps cross correlation time (CCT) is measured for the ω_1 and ω_s pulses. The bandwidth of the Stokes laser (ω_s) is ~700 cm^{-1}, and the spectral resolution of the CCD array (i.e., distance between two, wavelength-dispersed data points) is <0.5 cm^{-1}. The overall spectral resolution is limited by the bandwidth of the ω_1 laser pulse and is estimated to be <2 cm^{-1}. The upper limit on the error with which a band position can be determined is <1 cm^{-1} for Rh7.10 spectra throughout the 700−1700-cm^{-1} range.

Three, independently-operated optical delay lines are used to determine the timing sequence with which the three, picosecond dye laser pulses arrive at the liquid sample jet. Time delays between the pump pulse (ω_p) and the two probe pulses (ω_1 and ω_s) can be controlled over the 0.1-ps to 1-ns range via optical delay. In order to generate CARS signals, the phase-matching geometry of the **k** vectors for the ω_1 and ω_s laser beams are selected quantitatively by the beam steering optics.

The relative percentage of the Rh7.10 sample optically excited is estimated to be as high as 33% (derived from the intensity decrease in the 955-, 1235-, and 1551-cm^{-1} bands assigned to Rh7.10). The $\chi^{(3)}$ analysis of these Rh7.10 spectra requires normalization to the nonresonant background CARS signal. The measured instrumental response encompasses the spectral characteristics of all optical components used in the CARS experiments including the Stokes laser bandwidth (~20 nm, FWHM) which is sensitive to the stability of the Nd:YLF laser output. Both the nonresonant background and the spectral response can be readily determined by (i) simultaneously recording CARS spectra from the flowing jet sample and the reference at the beginning of each experiment and (ii) recording the spectra from the Rh7.10 sample and the water reference simultaneously throughout a complete set of picosecond resonant CARS (PR/CARS) and PTR/CARS measurements. The temporal overlap of the ω_1 and ω_s laser pulses is determined via autocorrelation measurements. The respective CCT traces are monitored on an oscilloscope to establish the ±2-ps error. The $\chi^{(3)}$ function used to fit each set of CARS data is performed using

(32) Ujj, L.; Volodin, B. L.; Popp, A.; Delaney, J. K.; Atkinson, G. H. *Chem. Phys.* **1994**, *182*, 291.

(33) Ujj, L.; Popp, A.; Atkinson, G. H. *Chem. Phys.* **1994**, *188*, 221.

(34) Ujj, L.; Jäger, F.; Popp, A.; Atkinson, G. H. *Chem. Phys.* **1996**, *212*, 421−436.

(35) Ujj, L.; Jäger, F.; Atkinson, G. H. *Biophys. J.* **1998**, *74*, 1492−1501.
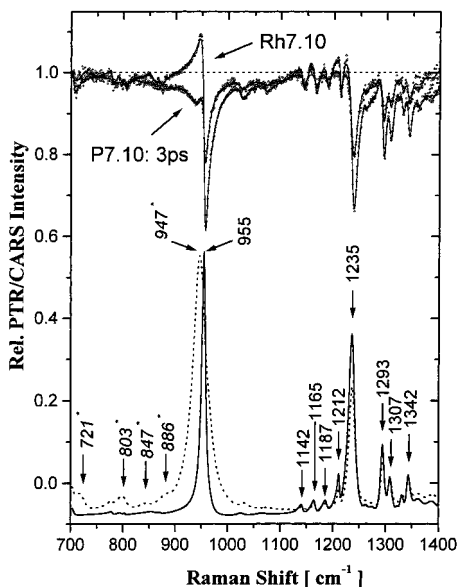
Figure 2. (Top) PR/CARS spectrum (700−1400 cm^{-1}) of Rh7.10 displayed together with the PTR/CARS spectrum indicating the presence of the P7.10 intermediate recorded 3 ps after the 3-ps, 500-nm excitation of Rh7.10. The respective $\chi^{(3)}$-fit functions are plotted as solid lines on top of the CARS data. (Bottom) Respective CARS spectra for Rh7.10 (solid line) and P7.10 (dotted line) without the $\chi^{(3)}$ background susceptibility and with Lorentzian line shape functions are presented. Only selected band positions are shown. The band positions of all significant features in these spectra are presented in Table 1. The most prominent P7.10 vibrational bands are marked with an asterisk over the HOOP region.

an Origin 4.1 program (Microcal Software Inc., Northamtpon, MA). The χ^2 error function, derived from a Levenberg−Marquardt approximation, is minimized as part of the $\chi^{(3)}$ fitting procedure.

Results

The seven-membered ring retinal (Figure 1, ref 7) has been shown by ultraviolet/visible absorption and circular dichroism spectra to occupy the same binding site in Rh7.10 as 11-*cis* retinal does in native Rh.[8,15,31] The PR/CARS spectrum of Rh7.10 shown in Figure 2 supports this conclusion *vide infra*. The $\chi^{(3)}$ fitting function is plotted over these data as a solid line, and the model function (after removing the interference with the background susceptibility) based on Lorentzian line shapes is displayed at the bottom of Figure 2.

Transient absorption data suggest that Rh7.10, unlike native Rh, does not form any photochemical products that comprise a photoreaction, but rather produces an apparent photophysical intermediate having a red-shifted absorption spectrum and a lifetime of <50 ps.[8,15] The PTR/CARS data presented here show that 20 ps after optical excitation, essentially all (>98%) of the Rh7.10 has been reformed. PTR/CARS measurements at 50-ps and 1-ns delays reveal spectra that are identical to the PR/CARS spectrum of Rh7.10 (i.e., without optical excitation). No secondary photochemistry is detected in these PTR/CARS data.

The vibrational spectrum of the P7.10 over the 700−1700 cm^{-1} region can be derived from PTR/CARS data recorded from the reactive mixture created by 3-ps, 500-nm excitation (e.g., the sample contains ∼33% P7.10 for data presented in Figure 2). The solid line in Figure 2 (bottom) is the Lorentzian fit to the Rh7.10 spectrum while the dotted line is the analogous fit to the P7.10 spectrum. To facilitate comparisons, the amplitudes of the 955- and 946-cm^{-1} bands in the respective P7.10 and
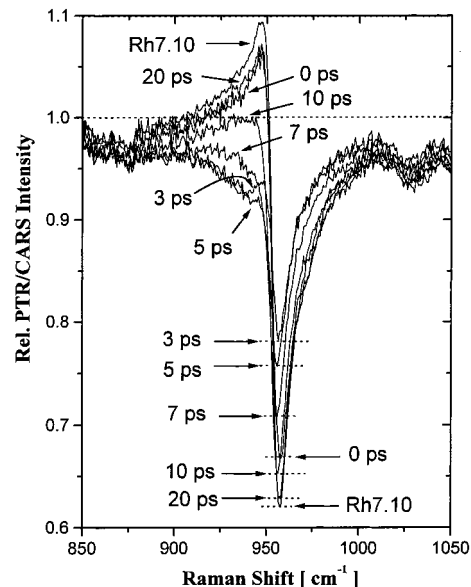

Figure 3. PTR/CARS data (850−1050 cm^{-1}) recorded at 0- (8-ps CCT), 3-, 5-, 7-, 10-, and 20-ps time delays (following 3-ps, 500 nm excitation of Rh7.10) showing the time-dependent intensity changes assigned to the prominent 955-cm^{-1} band. PR/CARS data from Rh7.10 alone are also presented for comparisons.

Rh7.10 Lorentzian spectra are normalized to each other. The correct ratio of concentrations is estimated to be ∼1.5 in favor of P7.10. A similar band amplitude relationship is observed for C=C stretching modes in native batho^{RT}.[28] The respective band positions can be regarded as accurate to within 1 cm^{-1}.

The PTR/CARS results presented here confirm the absence of an Rh7.10 photochemical reaction and the presence of the photophysical intermediate P7.10 although with a significantly different lifetime than that reported earlier.[8,15] These are, of course, the first vibrational spectra available for Rh7.10 and P7.10. The effect of optical perturbation on a protein sample such as Rh7.10 by the probe pulses (600 nm, 2.5 nJ, and ∼625−668 nm, 4.5 nJ) can be determined by methods similar to those used in the detailed studies of the BR photocycle.[32,34] Specifically, the upper limit for the probe laser perturbation is <5% of the total signal if 50% of the reactive mixture is comprised of P7.10. The irreversible degradation of the Rh7.10 sample after completing a set of measurements (i.e., ∼20 individual CARS spectra) is <5% and comparable to analogous measurements on BR-570.[34]

The most significant changes in the vibrational spectra of Rh7.10 and P7.10 are found in the 955-cm^{-1} band which is measured by PTR/CARS data at time delays from 0 ps (8-ps CCT) to 20 ps. The amplitudes of negative band intensities, which approximately represent the degree of optical bleaching in Rh7.10, are indicated for each time delay by horizontal arrows (Figure 3). The largest spectral change appears on the low-energy shoulder of the 955-cm^{-1} band in the 3-ps PTR/CARS spectrum. The $\chi^{(3)}$ fits to the PTR/CARS spectra recorded at 0-, 5-, 7-, 10-, and 20-ps delays monitor reaction mixtures with varying Rh7.10 and P7.10 concentrations and show that there exists a *continuous* change in the positions of the features corresponding to the 955-cm^{-1} band assigned to Rh7.10. The largest change in band position (Figures 2 and 3) indicates the presence of a 936-cm^{-1} band assignable to P7.10 (0-ps delay data). The corresponding bandwidths and the Θ values also are observed to undergo continuous change as a function of delay time. These results are derived for $\chi^{(3)}$-fit functions that are in excellent agreement with the PTR/CARS data. The value
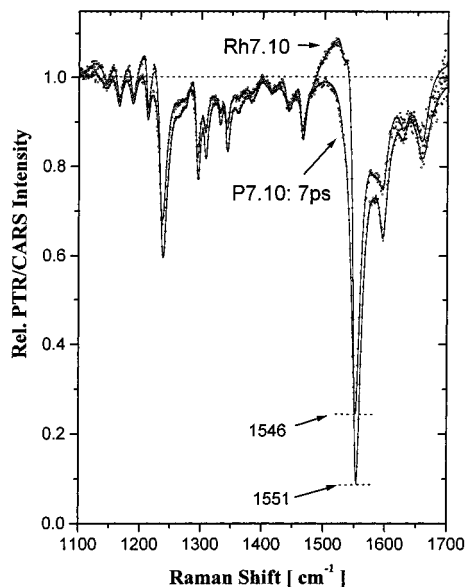
Figure 4. PR/CARS spectrum (1100−1700 cm^{-1}) of Rh7.10 displayed together with the PTR/CARS spectrum indicating the presence of the P7.10 intermediate recorded 7 ps after the 3-ps, 500-nm excitation of Rh7.10. The respective $\chi^{(3)}$-fit functions are plotted as solid lines on top of the CARS data.

Figure 5. Respective CARS spectra for Rh7.10 (solid line) and P7.10 (dotted line) without the $\chi^{(3)}$ background susceptibility and with Lorentzian line shape functions. Only selected band positions are shown. The band positions of all significant features in these spectra are presented in Table 1.

Table 1. Parameters (Ω_k Band Origin Positions, Γ_k Bandwidth (HWHM), and A_k Amplitudes) Derived from $\chi^{(3)}$ Fits to PR/CARS Data (700−1700 cm^{-1}) Assigned to Rh7.10 (Figures 2−5)[a]
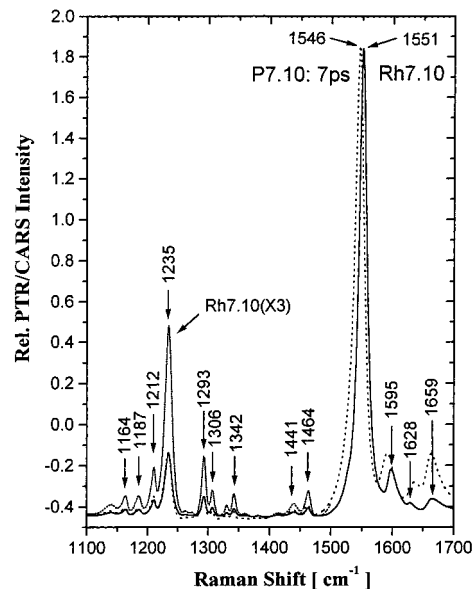
Ω_k (cm^{-1})	Γ_k (cm^{-1})	A_k	Ω_k (cm^{-1})	Γ_k (cm^{-1})	A_k
704	5	0.066	1293	4.5	0.21
779	4	0.029	1307	5	0.13
795	4	0.020	1322	4	0.03
804	2.5	0.024	1330	4	0.08
858	11	0.021	1342	4.5	0.13
872	4	0.013	1360	10	0.062
955	4.5	0.46	1382	9	0.060
964	7	0.041	1414	12	0.057
1026	8	0.034	1441	10	0.073
1070	15	0.027	1464	6	0.11
1103	15	0.009	1480	8	0.014
1142	4	0.056	1529	6	0.043
1165	4.5	0.071	1551	8	1.0
1187	5	0.057	1580	8	0.049
1212	2.5	0.093	1596	8	0.18
1235	7	0.37	1627	6	0.040
1262	6	0.039	1659	12	0.10
1273	9	0.049			

[a] The values for the PR/CARS amplitudes (A_k) are normalized to the amplitude of the 1551-cm^{-1} band.

of Θ, determined by the electronic absorption properties, is measured as 47° ± 10° for Rh7.10 and ∼130° ± 20° for P7.10 (i.e., maximum change at 3-ps delay).

PR/CARS data from Rh7.10 and PTR/CARS spectra of P7.10 recorded 7 ps after 3-ps, 500-nm excitation are presented in Figure 4 for the C−C stretching region (1100−1700 cm^{-1}). The $\chi^{(3)}$ fits, displayed as solid lines over these CARS data, are in excellent agreement with the CARS signal. The corresponding $\chi^{(3)}$ fitting parameters are presented in Table 1. The respective $\chi^{(3)}$ functions, without nonresonant backgrounds and with Lorentzian band shapes, are also displayed in Figure 5.

PTR/CARS data for the C=C stretching region for time delays from 0 to 20 ps are shown in Figure 6. The degree of optical conversion of Rh7.10 into P7.10 is indicated by the respective intensity levels. The 7-ps spectrum reveals a large spectral change on the low-energy shoulder of the 1551-cm^{-1}
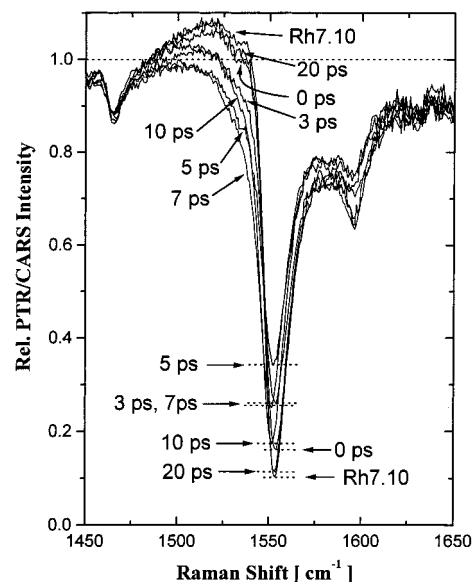
Figure 6. PTR/CARS data (1450−1650 cm^{-1}) recorded at 0- (8-ps CCT), 3-, 5-, 7-, 10-, and 20-ps time delays (following 3-ps, 500 nm excitation of Rh7.10) showing the time-dependent intensity changes assigned to the prominent 1551-cm^{-1} band.

band assigned to Rh7.10. The corresponding $\chi^{(3)}$ fitting parameters are presented in Table 1.

The most evident changes in these vibrational spectra involve the frequency decrease of the C=C stretching band from 1551 to 1546 cm^{-1} (Figure 4) which is accompanied by the maximum shift of Θ values from 53° ± 10° (Rh7.10) to 125° ± 20° (P7.10). Together with the results from the HOOP/fingerprint region, a shift of 72−83° in Θ for P7.10 is estimated. As a source of comparison, the 30-nm shift observed during the native Rh^{RT} to batho^{RT} transformation corresponds to a change in the Θ value of ∼100°.[28] The PTR/CARS results for Θ suggest that the formation of P7.10 involves a smaller (<25 nm) red shift in the absorption maximum than the 80-nm shift reported previously from transient absorption data identifying the 580-

nm species.[8,15] As for the HOOP/fingerprint region, a *continuous* shift of the C=C stretching band position and of the Θ value has to be considered in order to fit the $\chi^{(3)}$ susceptibility for all time delays measured in the respective PTR/CARS data.

Discussion

Three issues central to an understanding of the molecular mechanisms underlying the photoreactions of both Rh7.10 and native Rh[RT] can be addressed from the vibrational Raman spectroscopy of Rh7.l0 and its P7.10 intermediate: (i) the accurate identification of structural changes in the retinal that occur as P.710 is formed from Rh7.10, (ii) the time-dependent properties of the P7.10 structure as viewed in terms of its vibrational degrees of freedom, and (iii) the relationship(s) of the structural changes involved in P7.10 formation and the molecular mechanism underlying energy/storage in native Rh[RT] (vision). The first issue involves the band assignments to specific vibrational retinal modes and relies on analogous results from the vibrational spectroscopy of other retinal-containing proteins. The second issue analyzes the time-dependent CARS data in terms of specific vibrational modes. The third issue encompasses an elucidation of those dynamical and structural properties of P7.10 that can be related directly to the photo and batho intermediates found in the Rh[RT] photoreaction.

1. Vibrational Structures of Rh7.10 and P7.10. a. Assignments in the HOOP Region. The appearance of the 955-cm^{-1} band as a strong feature in the HOOP region of the P7.10 spectrum demonstrates the importance of the out-of-plane vibrational motions and the presence of a highly twisted P7.10 retinal structure. This is the major vibrational difference between the structures of Rh7.10 and P7.10. The precise vibrational mode assignment of the 955-cm^{-1} band requires an understanding of related assignments in native Rh[RT].

In native Rh[RT], the $HC_{11}=C_{12}H$ (A_2) HOOP mode appears at 970 cm^{-1} and is thought to have an especially high intensity due to the steric interactions of the $C_{13}-CH_3$ group with the hydrogen at C_{10} ($C_{10}-H$).[36-38] In general, HOOP modes *trans* to a C=C bond couple strongly to each other, thereby generating both in-phase (A_u) and out-of-phase (B_g) normal modes that have been assigned to bands appearing at $\sim$960 and $\sim$830 cm^{-1}, respectively.[38,39] Some specificity in such assignments can be found in native Rh[RT] since the CH_3 groups at C_9 and C_{13} divide the hydrogen-wagging motion into three categories: (i) C_7-H and C_8-H, (ii) $C_{10}-H$, $C_{11}-H$, and $C_{12}-H$, and (iii) $C_{14}-H$, $C_{15}-H$, and $N-H$.

The similarity of their respective Raman spectra strongly suggests that not only do both native Rh and Rh7.10 contain an 11-*cis*-retinal (*vide supra*), but that the remaining, more detailed vibrational assignments in native Rh[RT] have valid analogues in Rh7.10. Of the structural differences between native Rh[RT] and Rh7.10, the most important is the rigidity of the $C_{10}-C_{11}=C_{12}-C_{13}$ bonds within the 11-*cis*-retinal introduced by the seven-membered ring (Figure 1).

Structurally, the isomerization of 11-*cis* retinal around the $C_{11}=C_{12}$ bond, found to be of fundamental importance in the

native Rh[RT] photoreaction,[40] cannot occur in Rh7.10. In view of these PTR/CARS results (*vide infra*), transitory twisting of the $C_{10}-C_{11}=C_{12}-C_{13}$ bonds within the 11-*cis*-retinal previously proposed[9,15] appears to occur. Thus, the HOOP motions observed in P7.10, and therefore the assignment of the 955-cm^{-1} band, can be associated with the $HC_{11}=C_{12}H$ (A_u) HOOP mode.

Twisting elsewhere in the Rh7.10 retinal, of course, is not prevented. On the basis of the PTR/CARS data presented here (i.e., four new, low-intensity HOOP bands at 721, 803, 847, and 886 cm^{-1}), it is evident that the formation of P7.10 involves significant HOOP motion relative to that found in Rh7.10. The major indicator of HOOP motion is the shift of the vibrational band at 955 cm^{-1} to 936 cm^{-1} (Figures 2 and 7).

Of the three potential HOOP mode assignments for the observed 955-cm^{-1} band in Rh7.10 (i.e., $HC_7=C_8H$, $HC_{11}=C_{12}H$, and $HC_{15}=NH$ (Figure 1)), all can be considered as describing the twisting of P7.10 and have the requisite C=C *trans* structure. A detailed analysis of the Rh7.10 retinal geometry, including data from recently recorded vibrational Raman spectra of other Rh pigments containing artificial retinals (i.e., selective isotopic substitution and ring structures), only supports the assignment of the 955-cm^{-1} band to the $HC_{11}-C_{12}H$ HOOP mode.[41]

b. Assignments in the Fingerprint Region. The most prominent band appearing in the fingerprint region (containing primarily C—C stretching modes along the polyene chain) is at 1235 cm^{-1}. Other bands are observed at 1142, 1164, 1187, and 1212 cm^{-1}. These are to be compared with the PR/CARS spectrum of native Rh[RT] which contains bands at 1191, 1215, 1238, and 1268 cm^{-1}, the latter three of which have high intensities. The absence of the 1268-cm^{-1} band in Rh7.10 can be attributed to the incorporation of a seven-membered ring spanning the $C_{10}-C_{13}$ region (Figure 1).[41] In native Rh[RT], the 1268-cm^{-1} band has been assigned to the $HC_{11}-C_{12}H$ in-plane (A_1) wag. This assignment indicates that the modified geometry of the seven-membered ring retinal prevents in-plane motion of the hydrogens at C_{11} and C_{12}. There also appears a band at 1235 cm^{-1} (c.f. 1238 cm^{-1} in native Rh[RT]) of comparable intensity which can be assigned as the $C_{12}-C_{13}$ stretching mode although the $C_{14}-C_{15}$ stretching mode makes significant contributions.[37,41,42] The C_8-C_9 and $C_{14}-C_{15}$ stretching modes are expected to be relatively unaffected by the incorporation of the seven-membered ring in Rh7.10, and thus, each can be assigned to modes analogous to those found in native Rh[RT] (i.e., the 1212- and 1187-cm^{-1} bands, respectively).

The most important result to be derived from the vibrational degrees of freedom found in the fingerprint region is the confirmation that excitation of Rh7.10 does not alter the structure of the seven-membered ring nor any of the retinal modes encompassed by it. Specifically, the formation of P7.10 does not involve isomerization around $C_{10}-C_{11}=C_{12}-C_{13}$ bonds. The only noticeable changes in the fingerprint region appear on the low-energy side of the 1142- and 1212-cm^{-1} bands. Although not quantitatively analyzed, such changes suggest that, in addition to the twist of the $HC_{11}=C_{12}H$ bond, small amplitude motions appear within the seven-membered ring retinal.

c. Assignments in the Schiff Base ($C_{14}-C_{15}=N$) Region. Structural changes in the $C_{14}-C_{15}=N$ region are known to play important roles in the native Rh[RT] photoreaction, even though the retinal is sterically fixed at both the Schiff base linkage and

(36) Mathies, R. A.; Smith, S. O.; Palings, I. Determination of retinal chromophore structure in rhodopsins. In *Biological Applications of Raman Spectroscopy;* Spiro, T. G., Eds.; John Wiley & Sons: New York, 1987; Chapter 2, pp 59−108.

(37) Palings, I.; Pardoen, J. A.; van den Berg, E. M. M.; Winkel, C.; Lugtenburg, J.; Mathies, R. A. *Biochemistry* **1987,** *26*, 2544.
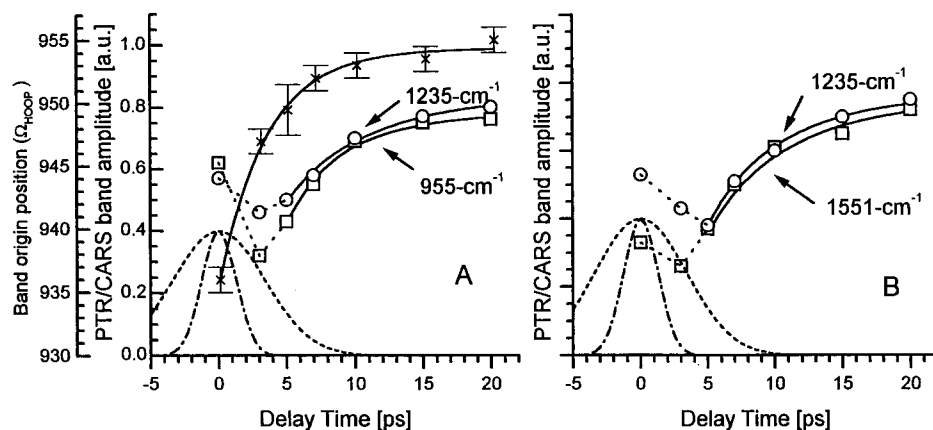
(38) Palings, I.; van den Berg, E. M. M.; Lugtenburg, J.; Mathies, R. A. *Biochemistry* **1989,** *28*, 1498.

(39) Eyring, G.; Curry, B.; Broek, A.; Lugtenburg, J.; Mathies, R. *Biochemistry* **1982,** *21*, 384.

(40) Wald, G. *Science* **1968,** *162*, 230.

(41) Zhou, Y.; Ujj, L.; Lou, J.; Jäger, F.; Nakanishi, K.; Atkinson, G. H. *J. Phys. Chem.*, submitted for publication.

(42) Ganter, U. M.; Gärtner, W.; Siebert, F. *Biochemistry* **1988,** *27*, 7480.

Figure 7. (A) Time evolution of the amplitudes (A_k) of the 955-cm^{-1} (HOOP; □ data) and 1235-cm^{-1} (C–C stretching; ○ data) CARS bands assigned to Rh7.10. The A_k values are derived from the $\chi^{(3)}$ fits to PTR/CARS spectra recorded in the 700–1400-cm^{-1} region. Single exponential, kinetic fits to these data lead to time constants of 0.9 ps (bleach) and 5.0 ps (recovery) for the 955-cm^{-1} band and 1.5 ps (bleach) and 6.0 ps (recovery) for the 1235 cm^{-1} band. Schematic representations of the pump (-·-) and pump/probe, CCT (- - -) laser profiles are shown. To minimize the effects of these laser profiles, only A_k values in the 5–20 ps interval are used to calculate these time constants. Time evolution of the origin position of the 955-cm^{-1} HOOP bands (Ω_{HOOP}; × data) assigned to P7.10 (band origin position scale shown on far left). These Ω_{HOOP} values are taken from the PTR/CARS spectra recorded in the 750–1050-cm^{-1} region. A single exponential, kinetic fit to these Ω_{HOOP} data leads to time constants of 5 ps for the increase from 936 to 955 cm^{-1}. (B) Time evolution of the amplitudes (A_k) of the 1235-cm^{-1} (C–C stretching; ○ data) and 1551-cm^{-1} (C=C stretching; □ data) CARS bands assigned to Rh7.10. The A_k values are derived from the $\chi^{(3)}$ fits to PTR/CARS spectra recorded in the 1100–1700-cm^{-1} region, and the vertical scale is the same as that shown in (A). Single exponential kinetic fits to these data lead to time constants of 1.0 ps (bleach) and 5.9 ps (recovery) for the 1235-cm^{-1} band and 1.1 ps (bleach) and 6.2 ps (recovery) for the 1551 cm^{-1} band. Schematic representations of the pump (-·-) and pump/probe, CCT (- - -) laser profiles are shown. To minimize the effects of these laser profiles, only A_k values in the 5–20 ps interval are used to calculate the time constants.

at the β-ionone ring.[43–45] The retinal in Rh7.10 is also fixed at the Schiff base linkage and the β-ionone ring, but in addition, motion throughout the C_{10}–C_{11}=C_{12}–C_{13} region is restricted by the seven-membered ring. Since only minor spectral changes are observed in the fingerprint region (Figures 2 and 4), there is no evidence suggesting that the C_{14}–C_{15}=N modes are involved in the enhancement of out-of-plane, torsional motion that is evident in the P7.10 retinal. The intensity increase observed in the 1659-cm^{-1} C_{15}=N band may be due to a different electronic configuration of the excited state of P7.10.

2. Kinetics Associated with Rh7.10 and P7.10. a. Transient Absorption and PTR/CARS Species. Although both are identified as intermediates formed by optical excitation of the same artificial Rh pigment, Rh7.10, the relationship between the 580-nm, 44-ps lifetime species observed by transient absorption[8] and P7.10 observed via PTR/CARS remains unclear since each has significantly different kinetic and absorption properties.

Given the 25-ps time resolution of earlier transient absorption measurements, the rise time of the 580-nm intermediate could not be resolved, although a decay time of 44 ps has been reported.[8] Essentially no fluorescence from this intermediate is reported.[8,15] The PTR/CARS spectra reported here are recorded with sufficient time resolution (3-ps pulse, 8-ps CCT) to confidently determine that P7.10 decays in <10 ps, but can be used only to estimate a formation time of ~1 ps. These apparent differences in kinetic properties can be attributed to the different experimental time resolution (25 ps versus 3 ps).

The differences in absorption maxima (580 nm[8] versus 525 nm [this work]), however, are more difficult to reconcile. A

comparison of excitation conditions based on the photon flux density[34] ($\xi = \sigma N_{ph}/A$, where σ is the absorption cross section and N_{ph}/A is the number of photons per excitation area) shows that approximately the same average number of photons per molecule (0.2 versus 0.3) is used in the two types of experiments, thus eliminating power-dependent effects. On the basis of the uncertainties in the earlier kinetic and spectral measurements, a conclusion on whether the same species is observed in both studies cannot yet be reached.

b. Formation and Decay Times. The transformations between Rh7.10 and P7.10 can be quantitatively characterized in terms of the intensity changes in the 955-, 1235-, and 1551-cm^{-1} PTR/CARS bands assigned to Rh7.10 and the change in maximum positions of the 936- and 955-cm^{-1} bands assigned to P7.10. The time-dependent band intensities and positions are based respectively on the A_k and Ω_k values derived from the $\chi^{(3)}$ fit to each PTR/CARS spectrum. The A_k and Ω_k values are presented as a function of reaction time in Figure 7 (A_k values for the 1235-cm^{-1} band are independently measured in two, separate spectral regions, Figures 2 and 5).

The kinetics describing the optical bleach (decrease) and recovery times for the Rh7.10 population are obtained from these data using separate, single exponential functions. The bleaching function is convoluted with the 8-ps (Gaussian) cross correlation function describing the two probe laser pulses. The bleaching and recovery times found for all three PTR/CARS bands from Rh7.10 are in excellent agreement (bleach of 1.1 ps/ recovery of 6.2 ps for 1551-cm^{-1} band; bleach of 0.9 ps/recovery of 5.0 ps for 955 cm^{-1} band; and bleach of 1.0 ps (C=C/C–C) and 1.5 ps (HOOP/C–C)/recovery of 5.9 ps (C=C/C–C) and 6.0 ps (HOOP/C–C) for 1235 cm^{-1} band).

A single exponential analysis of the time-dependent positions of the 936–955-cm^{-1} bands shows that the P7.10 population decreases with a 3.5-ps time constant (Figure 7A). Although the C=C stretching (1546–1551 cm^{-1}) bands also shift (Table

(43) Jäger, F.; Jäger, S.; Kräutle, O.; Friedman, N.; Sheves, M.; Hofmann, K. P.; Siebert, F. *Biochemistry* **1994**, *33*, 7389.

(44) Nakanishi, K.; Zhang, H. Z.; Lerro, K. A.; Takekuma, S.; Yamamoto, T.; Lien, T. H.; Sastry, L.; Baek, D.-J.; Moquin-Pattey, C.; Boehm, M. F.; et al. *Biophys. Chem.* **1995**, *56*, 13.

(45) Yan, B.; Takahashi, T.; McCain, D. A.; Rao, V. J.; Nakanishi, K.; Spudich, J. L. *Biophys. J.* **1990**, *57*, 477.

Table 2. Parameters (Ω Band Origin Positions and Θ Electronic Phase Factors) Derived from $\chi^{(3)}$ Fits for the C=C Stretching and HC$_{11}$=C$_{12}$H HOOP Modes Assigned to Either Rh7.10 or P7.10[a]

$\chi^{(3)}$ parameters	Rh7.10	P7.10						
		0 ps	3 ps	5 ps	7 ps	10 ps	15 ps	20 ps
Ω (C=C) (cm^{-1})	1551	1551	1550	1548	1546	1547	1547	1549
Θ (C=C) (deg)	53	56	68	95	125	95	89	69
Ω (HOOP) (cm^{-1})	955	936	947	947/952	952	953	953.5	955
Θ (HOOP) (deg)	47	61	116	128	129	118	105	110

[a] The values assigned to P7.10 are presented for seven different time delays as measured by PTR/CARS.

2), the 955-cm^{-1} band is the only PTR/CARS feature assigned to P7.10 that is strong enough to merit kinetic analysis.

The excellent agreement between the kinetic parameters assigned to Rh7.10 indicate that it is reformed from P7.10 as a vibrationally-equilibrated species. The difference between the 3.5-ps decay of P7.10 and the 6-ps reformation of Rh7.10, however, indicates that there is more than one molecular pathway leading to Rh7.10 following optical excitation. Since the Rh7.10 population is completely restored within 20 ps, the second pathway must have a lifetime comparable to that of the P7.10 to Rh7.10 pathway, i.e., <10 ps. A reasonable candidate is relaxation from the excited electronic state of Rh7.10 populated by absorption. Independent of these kinetic differences, the concentration parameters derived from the $\chi^{(3)}$ analysis indicate that a part of the Rh7.10 population is not present in the PTR/CARS signals recorded at 0, 3, and 5 ps, suggesting that some of the Rh7.10 population is not converted into P7.10 during this initial ∼5-ps interval. These data, therefore, can be viewed as establishing that the quantum yield for formation of P7.10 following optical excitation of Rh7.10 is less than unity.

c. Time Evolution of the P7.10 Vibrational Structure. Interest in the time-dependent vibrational structure of P7.10 obtains for two reasons: (i) the dynamics associated with the mechanism by which P7.10 is formed and (ii) determining its relationship to the transient structures of the photo[RT] and batho[RT] intermediates in the native Rh[RT] photoreaction.

Based on vibrational spectra, it is reasonable to conclude that the seven-membered ring retinal in Rh7.10 adopts a geometry similar to that of 11-*cis*-retinal in native Rh[RT] (i.e., 6-*s-cis*, 15-*anti*) as well as an analogous orientation in the binding pocket, *vide supra*. Differences may occur, however, in the ordering of alternating twisting along the conjugated retinal chain. For example, the out-of-plane distortions around the C$_{11}$=C$_{12}$ bond in native Rh[RT] are likely shifted within the seven-membered ring section, and the retinal C$_{10}$—C$_{11}$=C$_{12}$—C$_{13}$ bond lengths in Rh7.10 may be stretched in order to accommodate the seven-membered ring (Figure 1).

The distinct time evolution of the P7.10 structure can be elucidated from an examination of the band positions (Ω) and Θ values for the prominent CARS features (Table 2). The monotonic changes in the Ω and Θ values observed as a function of reaction time (0−20 ps in Table 2) strongly suggest that the P7.10 structure evolves *continuously* throughout the initial 20 ps.

It is important to recall that the relationship between Θ and the absorption band maximum for a given species derives from the $\chi^{(3)}$ function used to model the CARS data.[46,47] Each Θ value presented here is derived from an excellent $\chi^{(3)}$ fit for features within a spectral region (e.g., 700−1400 cm^{-1}).

The data presented in Table 2 show that between 0−20-ps delays there exists a continuous change in the frequency positions of the 955-cm^{-1} HOOP and 1551-cm^{-1} C=C bands which is accompanied by a continuous change in Θ values. The correlation between Θ values and the frequencies of the HC$_{11}$=C$_{12}$H HOOP and C=C stretching modes indicates that the *continuous* structural changes in P7.10 over the initial 20 ps are accompanied by an analogous *continuous* change in the P7.10 absorption maximum.

Collectively, the constancy of the Schiff base environment, the red-shifted absorption maxima (via Θ values), and the changes in HOOP and C=C band positions can be interpreted in terms of a twisting at C$_{11}$=C$_{12}$ which does not significantly alter the distance between the retinal and either the Glu-113 counterion or the Schiff base nitrogen.

3. Implications for the Energy Storage/Transduction Mechanism in Rh[RT]. This analysis of these PTR/CARS data suggests that the formation of P7.10 following the optical excitation of Rh7.10 involves primarily motion along the C$_{11}$=C$_{12}$ (*cis−trans*) reaction coordinate found to be active in native Rh[RT]. The dynamic analysis reveals continuous evolution of twisted, out-of-plane structures that are primarily restricted to torsional motion around the C$_{11}$=C$_{12}$ bond. This result supports the conclusion that the 11-*cis* to all-*trans* isomerization in Rh[RT] is an essential reaction coordinate in vision and the primary structural pathway leading to stable, ground-state Rh[RT] intermediates (e.g., batho[RT]).

The excellent correlation between the continuous evolution of absorption maxima and frequency of the nonreactive C$_{11}$=C$_{12}$ coordinate in P7.10 indicates that the π-electron delocalization changes within the retinal structure as P7.10 forms and decays. Thus, the time scales for electronic and vibrational relaxation within Rh7.10 and P7.10 appear, to within an order of magnitude, to be about the same.

The broadening of the 936−955-cm^{-1} features (C$_{11}$=C$_{12}$ HOOP mode) observed for P7.10 may also be associated directly with the continuous out-of-plane motion.

The current model describing energy storage/transduction in Rh[RT], based on femtosecond time-resolved, differential absorption data (570 and 630 nm), reveals a 200-fs process which has been interpreted as a coherent vibrational motion along the C$_{11}$=C$_{12}$ reaction coordinate.[3,4] This reaction coordinate has been associated with a 60-cm^{-1} torsional motion within the retinal polyene structure. Analogous studies show that *cis/trans* isomerization in 9-*cis*-Rh[48] slows to 600 fs and in 13-demethyl-11-*cis*-rhodopsin[49] slows to 400 fs. These femtosecond processes also can be detected via excited-state lifetime measurements: 50 fs for 11-*cis*-Rh[11] and 100 fs for 9-*cis*-Rh.[11] It has been concluded that the same vibrational coherent relaxation underlies the initial steps in these respective Rh pigments, namely, the formation of photo[RT] with its red-shifted absorption maximum.

(46) Oudar, J.-L.; Shen, Y. R. *Phys. Rev. A* **1980**, *22*, 1141.

(47) Mukamel, S. *Principles of Nonlinear Optical Spectroscopy*; Oxford University Press, Inc.: New York, 1995.

(48) Schoenlein, R. W.; Peteanu, L. A.; Wang, Q.; Mathies, R. A.; Shank, C. V. *J. Phys. Chem.* **1993**, *97*, 12087.

(49) Wang, Q.; Kochendörfer, G. G.; Schoenlein, R. W.; Verdegem, P. J. E.; Lugtenburg, J.; Mathies, R. A.; Shank, C. V. *J. Phys. Chem.* **1996,** *100*, 17388.

Thus, this model suggests that nonstationary, excited vibrational states play important roles in all of the respective isomerization dynamics. It must be noted, however, that only transient absorption data containing no direct information on vibrational structure have been used as a basis for these interpretations.

A different type of dynamics appears to be present in Rh7.10. The increase in Θ values, corresponding to red-shifted absorption maxima, does not result in a *cis/trans* isomerization nor the formation of a new, stable photoproduct (e.g., batho[RT]) nor a change in the distance between the protonated Schiff base nitrogen and the Glu-113 counterion. All of these phenomena have been suggested as the molecular change underlying the red-shifted absorption observed in other Rh pigments and, thereby, used to distinguish and identify the molecular properties of intermediates such as photo[RT]. While some or all of these properties may pertain to photo[RT] in the Rh[RT] photoreaction (as well as in other Rh pigments), it is evident from these PTR/CARS data on Rh7.10 and P7.10 (where none of these processes occur) that a red-shifted absorption maximum does not necessarily signify the presence of a photo[RT] species. Rather, red-shifted, transient absorption may only reflect the energy difference between the electronically excited- and ground-state wavepacket as it accelerates out of the FC region of the potential surface along the reaction coordinate. The maximum red shift is reached for the maximum distortion of the reaction coordinate (e.g., at ~90° torsion around a classical $C=C$ isomerization reaction coordinate) and the associated change in π-electron delocalization within the retinal. Torsional motion around $C_{11}=C_{12}$ in Rh7.10 represents such a case. If the torsional distortion cannot proceed beyond a certain point in the reaction coordinate, however, isomerization cannot be completed (i.e., a stable intermediate such as batho is not formed).

The molecular mechanism underlying the formation of P7.10 from Rh7.10 (derived from PTR/CARS data) is consistent with that proposed for the Rh[RT] photoreaction. By eliminating the 200-fs, $C_{11}=C_{12}$ isomerization reaction coordinate, the Rh7.10/P7.10 photoreaction provides an opportunity to determine if other reaction coordinates exist within retinal. There is no evidence, however, to suggest that a reaction coordinate in Rh7.10 leads to a stable intermediate such as batho[RT], but there are reasons to conclude that "photo-like" properties are found in P7.10, namely, rapid (fs/ps), red-shifted absorption (*vide supra*).

Since the transient, red-shift absorption mimics that of photo[RT], it is interesting to consider whether the vibrational structure found in P7.10 from PTR/CARS data has relevance to the unknown vibrational structure of photo[RT]. Although it is clear that isomerization around the $C_{11}=C_{12}$ bond is accompanied or preceded by the <1-ps, red-shifted absorption used to identify photo[RT], there is no evidence to support the earlier conclusion that isomerization of the $C_{10}-C_{11}=C_{12}-C_{13}$ moiety *causes* the observed red-shifted absorption.[8] The PTR/CARS data presented here demonstrate that a red shift in absorption can occur independently of $C_{11}=C_{12}$ isomerization, and therefore, these PTR/CARS results do not support the characterization of photo[RT] as necessarily involving motion in the $C_{10}-C_{11}=C_{12}-C_{13}$ bonds, including $C_{11}=C_{12}$ isomerization.

Concluding Remarks

The PTR/CARS methodology is successfully applied to an artificial Rh pigment obtained by the regeneration of opsin with a chemically-modified retinal containing a seven-membered ring spanning C_{10} to C_{12} (Rh7.10) in which the isomerization around the $C_{11}=C_{12}$ bond is blocked (Figure 1). Optical excitation of Rh7.10 generates within <1 ps a single intermediate (P7.10) which has a retinal structure distinct from that of Rh7.10. Solely on the basis of the analysis of vibrational degrees of freedom (i.e., PTR/CARS data), P7.10 can be viewed (i) as the only product formed by optical excitation of Rh7.10, (ii) as decaying completely back to Rh7.10 with a time constant of about 6 ps (>98% reformed after 20 ps), and (iii) as representing a series of intermediates having distinct, but well-defined structures involving different degrees of the out-of-plane motion around the $C_{11}=C_{12}$ retinal bond. These PTR/CARS data indicate that the seven-membered, 11-ene ring is flexible enough to permit significant motion either within the ring itself or along the $C_{11}=C_{12}$ reaction coordinate or both, but that *no* 11-*cis* to all-*trans* isomerization occurs in R7.10.